CHEMISTRY OF MATERIALS

ARTICLE

pubs.acs.org/cm

Enhancing Electronic Conductivity in Strontium Titanates through Correlated A and B-Site Doping

Dragos Neagu* and John T. S. Irvine

School of Chemistry, University of St Andrews, North Haugh, St Andrews, Fife KY16 9ST, U.K.

ABSTRACT: A doping strategy aimed at improving n-type conductivity in perovskite oxides by enhancing bulk oxide ion mobility is proposed and discussed. To justify and further assess this premise, the oxygen deficiency (δ) and conductivity (σ) of reduced $La_{0.4}Sr_{0.4}Ga_xTi_{1-x}O_{3-x/2-\delta}$ ($0 \le x \le 0.15$) samples were studied as a function of Ga doping (x). Both δ and σ were found to increase significantly with Ga doping. After a typical reduction process carried out at 1000 °C in 5%H_2/Ar the samples showed an increase in δ from 0.035 to 0.060 with doping. The corresponding conductivity also increased with doping showing a maximum of ~50 S cm^{-1} (measured at 880 °C in 5% H_2/Ar on ~62% dense pellet) for x = 0.05. Conductivity data suggests Ga doping promotes fast reduction and significantly improves the stability of the reduced phase in oxidizing conditions. Although the studied compositions preserved their cubic crystal structure throughout testing and showed no sign of degradation of the microstructure, some Ga loss was shown to take place at low pO_2. However, after a first redox cycle, no further change in Ga stoichiometry was observed. Two mechanisms that account for the manner in which Ga is lost from the perovskite lattice are proposed and discussed.

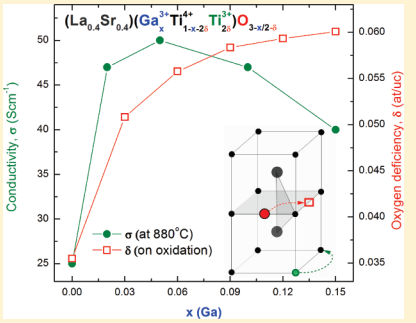

KEYWORDS: perovskites, strontium titanate, doping, oxygen deficiency, conductivity

1. INTRODUCTION

Metal oxides with ABO_3 stoichiometry and cubic structure are generally known as perovskite oxides. In the regular perovskite lattice the smaller B-site ions occupy the corners of a cube in 6-fold oxygen coordination forming BO_6 octahedra (Figure 1a). The larger A-site ions are positioned in the center of the cube in 12-fold coordination. Because of the exceptional tolerance of the perovskite structure to accommodate different cations and defects, the perovskite family consists of a large number of compounds and displays a wide variety of properties.[1]

Among other properties exhibited by the perovskite structure and currently under investigation, electronic and ionic conduction are of interest because of both scientific and application potential. The development of materials with very high electronic conductivity or with mixed electronic and ionic conduction (MIEC) is of great interest for the advance of high temperature electrochemical devices.

Generally, electronic conduction in perovskites occurs through the B-site network when these sites are occupied by cations capable of adopting multiple oxidation states (Ti^{4+}/Ti^{3+}, Nb^{5+}/Nb^{4+}, Mn^{4+}/Mn^{3+}, etc). Conduction most likely occurs because of electron hopping from $B^{(n-1)+}$ cations to B^{n+} cations via the oxygen bridges (similar to a double exchange mechanism), as shown schematically in Figure 1b. The higher the concentration, $[B'_B]$, and the mobility, μ_{e^-},of the charge carriers (e^-), the higher the conductivity, σ_{e^-}:

$$\sigma_{e^-} = [B'_B] \cdot e \cdot \mu_{e^-} \quad (1)$$

Most of the strategies aimed at designing good electronic conductors focused on increasing the concentration and/or the mobility of the charge carriers. The mobility of the electrons depends mainly on the crystal structure (present ions, size, and symmetry/distortion of the unit cell) and the microstructure of the sample (usually the higher the number of grain boundaries, the lower the conductivity). The generation of electrons is usually promoted by appropriate doping and/or (more often) by exposing the materials to a reducing environment which strips oxygen ions from the structure and subsequently reduces B^{n+} to $B^{(n-1)+}$:

$$2B_B^x + O_O^x \leftrightarrow 2B'_B + V_O^{\cdot\cdot} + \frac{1}{2}O_2 \quad (2)$$

The process described by eq 2 usually occurs fast at the surface of ceramics (at the solid−gas interface) and slower and slower as the reduction proceeds into the bulk.[2] This happens essentially because oxide ions need to travel through the bulk before being oxidized at the surface by reacting with the gas phase. This is why the reduction of this kind of material, carried out at typical testing temperatures (~900 °C), was often reported to take tens of hours, especially for samples with low porosity.[3−5] Because the transport of oxide ions through the bulk appears to be the rate determining step in the reduction process, limiting the rate and extent of the reduction, it is worth identifying the key factors that influence it. A good image of how oxygen transport through the perovskite lattice takes place can be acquired by looking at oxide ion conduction in some perovskites, such as doped lanthanum gallates, for which a large volume of literature data is available.[6−14]

Received: December 7, 2010
Revised: January 21, 2011
Published: February 11, 2011

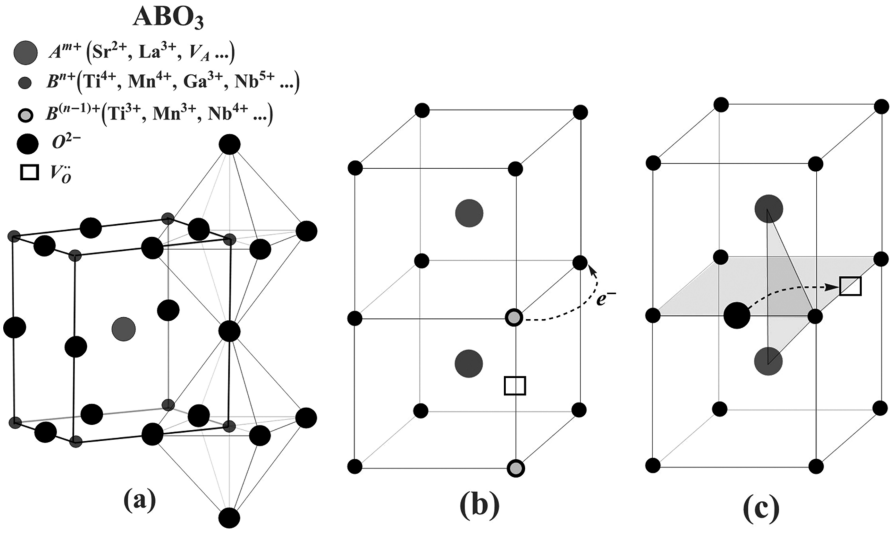

Figure 1. (a) Unit cell of perovskite-type oxide together with some typical cations that occupy the A and B sites. (b) Schematic view of the electronic conduction in perovskites. The oxygen lattice is omitted for clarity. (c) Schematic view of the oxide ion conduction in perovskites. Most of the oxygen ions are omitted for clarity.

Similar to the electronic conduction, available hopping sites for the charge carrier, which in this case is O^{2-}, are necessary for oxide ion conduction to take place. When the concentration of oxygen vacancies is high enough, oxide ion conduction can occur through the crystal. Previous studies have shown that probably the most important stage in this process is when the oxide ion must move through the bottleneck defined by the triangle A-B-A to reach the vacant site[7,10,12,13] (Figure 1c). The diffusion of the oxide ion through the crystal can be synthetically expressed as follows:[10]

$$D_{O^{2-}} \sim [V_O^{\cdot\cdot}] \cdot a^2 \cdot e^{-(\Delta Hf + \Delta Hm + \Delta Ha)/(R \cdot T)} \quad (3)$$

Equation 3 shows that diffusion is proportional to the concentration of *mobile* vacancies, $[V_O^{\cdot\cdot}]$, and the square of the cell parameter, *a*. Diffusion also depends on three main processes and their associated thermal effects: formation (ΔH_f), migration (ΔH_m), and association (ΔH_a) of vacancies. The way these factors come into play can be better understood by studying Figure 1c. When the oxide ion starts moving from its position it will need to break the bond shared with one of the adjacent B cations (the A−O bonds are generally very weak compared to the B−O bonds). Moreover, when the bond breaks the corresponding B cation will decrease its coordination number from 6 to 5. Most of the B-site cations form strong bonds with oxygen and strongly prefer 6-fold coordination; therefore, the energy required for the formation of the vacancy, ΔH_f, is high. Some cations, such as Mn, Co, Ga, and so forth, are known to be stable in coordination numbers lower than 6 as well[15] and have been successfully employed in the design of materials with good electronic and ionic conduction.[16,17] To reach the vacant site, the oxide ion will have to migrate through the triangle described by the two A-site cations and the B-site cation. Among the factors that come into play during this stage, the most important are the nature (electronic structure, size, etc.) of the A-site cations and the distortions of the lattice which can prevent the oxide ion from taking the simple path indicated in Figure 1 c. The most important parameter controlling the migration of the oxide ion is the degree of distortion from a lattice exhibiting high symmetry and little stress, in which the oxide ion was found to possess the highest mobility for vacancy hopping.[7,11,13] Usually the migration energy is smaller compared to the vacancy formation energy.[10] Other processes such as the association (trapping) of oxygen vacancies with other oxygen vacancies and/or other defects can impair diffusion.[10,11,18] Usually this results in the mobile vacancy concentration being smaller than the stoichiometric one. Typical cases of such associations are oxygen vacancy ordering or the association of the oxygen vacancy with A-site dopants. When oxygen vacancy ordering occurs, ionic conductivity significantly diminishes,[7,8] or the reduction rate of the material is significantly affected;[19] therefore, a random distribution of these vacancies throughout the crystal is to be desired. When the A-site ion is partially substituted by another ion, oxygen vacancy trapping can occur, mostly because of size mismatch between the host and the substitution ion.[18] Where the size of the host and dopant are similar, for example, when substituting Sr^{2+} (1.44 Å) for La^{3+} (1.36 Å) in lanthanum gallates, ΔH_a has been calculated to be zero.[18]

The aim of this work is to show that perovskite systems that rely on eq 3 to achieve high electronic conductivity will benefit from having a good oxide ion transport throughout the lattice. If oxygen transport is high, the material could also exhibit some ionic conduction and thus be potentially mixed ionic and electronic conductors (MIECs). Therefore, generally speaking, the best electronic conductors would be mixed electronic conductors.

In the light of the arguments described above we chose as starting point a material that we investigated in our previous study;[2] a cubic, A-site deficient titanate ($La_{0.4}Sr_{0.4}TiO_3$) which we showed to suffer from slow bulk reduction. We chose Ga as B-site dopant for several reasons. First, Ga is well-known for its coordination flexibility and the ability to increase the stability of systems with high oxygen deficiency. Second, Ga^{3+} has similar radius to Ti^{4+} across various coordination numbers suggesting it will be soluble in the titanate, as can be seen from Figure 2 where Shannon radii[20] are plotted against coordination number. Finally, by replacing Ti^{4+} with Ga^{3+} some oxygen vacancies will be created to compensate for this doping ($La_{0.4}Sr_{0.4}Ga_xTi_{1-x}O_{3-x/2}$), which together with the vacancies generated during reduction could support ionic conduction.

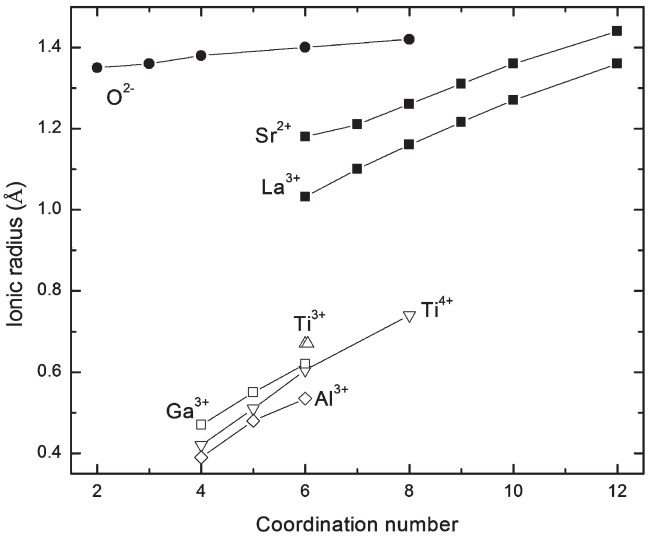

Figure 2. Ionic radii vs coordination number for some cations that can occupy the A and B site in a perovskite lattice. B-site cations have small radius and small coordination number, while A-site cations have large radius and high coordination number.[20].

According to eq 2, Ga doping will primarily affect two easily measurable properties: electronic conductivity and weight loss (oxygen deficiency) on reduction. Therefore this study will make use of these two parameters to assess the influence of Ga doping.

2. EXPERIMENTAL SECTION

2.1. Sample Preparation. The samples have been prepared by a modified solid state route. High purity raw materials (La_2O_3, $SrCO_3$, TiO_2, Ga_2O_3, and Al_2O_3) were dried, weighed, and mixed in the corresponding ratios in a beaker with acetone. An ultrasonic probe was then immersed into the beaker, and ultrasonic waves having different amplitudes and frequencies were applied to break the agglomerates into a fine suspension. A small quantity (~0.1%) of dispersant (KD1) was added to the suspension which was then stirred for 2 h. After the acetone has been evaporated, the content of the beaker was quantitatively transferred into a crucible and calcined at 1000 °C for 12 h. The calcined powder was then milled for 2.5 h in a planetary ball mill. The resulting powder was pressed into dense pellets and fired for 12−14 h at 1400 °C. The sintered pellets were crushed and ball-milled for 1.5−4 h (depending on the desired grain size). The fine, sintered powder was mixed with spherical glassy carbon, pressed into pellets, and fired slowly to 1390 °C. The initial ramp rate of the program was set at 2 °C/min until 1000 °C, to allow a slow burn-out of the carbon, and thus create pores in the ceramic bodies. The samples were then heated with 5 °C/min to the sintering temperature, 1390 °C, and kept there for 6 h. Porous pellets having a mass of around 1 g have been prepared this way for weight loss measurements. Reduction has been carried out in tubular furnaces under continuous 5%H_2/Ar flow.

2.2. Analysis Techniques. The crystal structure and phase purity of the samples were analyzed using X-ray diffraction (XRD) performed on either a STOE STADI Transmission Diffractometer (Cu$K\alpha_1$ radiation) or a Philips PW 1710 Reflection Diffractometer (Cu $K\alpha_1$, $K\alpha_2$ radiation). Silicon was used as internal standard in some of the runs. The obtained XRD patterns were analyzed with the STOE Win XPOW software to determine the crystal structure and the cell parameter. Rietveld refinement (using FullProf software) was also carried out for some samples. The microstructure of the samples was analyzed using a JEOL JSM-5600 Scanning Electron Microscope (SEM). Energy Dispersive X-ray (EDX) analysis was also employed in some of the cases to confirm the stoichiometry of the samples. Thermo-gravimetric analysis was performed using a Netzsch STA 449C instrument equipped with Proteus thermal analysis software. The total conductivity of the samples was measured using a DC, van der Pauw setup. To perform a measurement, 4 small strips of gold mesh were attached to the periphery of the sample using gold paste and fired at 850 °C for 1 h, to ensure the consolidation of the contacts. The sample was then mounted on the testing jig which is equipped with a thermocouple and a zirconia sensor in the vicinity of the sample so that the temperature of the sample and the oxygen partial pressure can be recorded. The jig was then inserted in a controlled atmosphere furnace. Low oxygen partial pressure is achieved by using a continuous flow of 5%H_2/Ar.

3. RESULTS AND DISCUSSION

3.1. Crystal Structure and Microstructure. The crystal structure and phase purity of the gallium doped titanates ($La_{0.4}Sr_{0.4}Ga_xTi_{1-x}O_{3-x/2}$) has been analyzed using room temperature powder XRD (Figure 3). All compositions up to x = 0.15 showed single phase, cubic ($Pm3m$) crystal structures. For x = 0.15 very small peaks corresponding to unreacted Ga_2O_3 were observed, suggesting the solubility limit of Ga in $La_{0.4}Sr_{0.4}TiO_3$ is between x = 0.10 and x = 0.15. The XRD patterns presented in Figure 3 were refined using Rietveld analysis to confirm the crystal structure and extract accurate cell parameters. The cell parameters plotted in Figure 4 seem to follow Vegard's law, increasing linearly with Ga doping. The fact that the cell parameters increase with doping was to be expected as we are substituting the smaller Ti^{4+} (0.605 Å) ion with the slightly larger Ga^{3+} (0.62 Å) ion as well as introducing vacancies.

Previously we have shown that an empirical equation adapted from fluorite systems[21] can be used to predict the slope of the cell parameter vs doping plot:[2]

$$a = a_0 + \sum_k x_k \cdot (\Delta r_k + 0.002 \cdot \Delta z_k) \qquad (4)$$

Equation 4 shows that a linear correlation should be expected between the cell parameter (a) and the mole fraction (x_k) of the cation k substituting the B-site host cation in a perovskite lattice. The slope will depend on the difference in the ionic radius (Δr_k) and charge (Δz_k) between the substituting cation k and the host cation. In this case Δr = 0.015 and Δz = −1, predicting a slope of 0.013, while the slope obtained from experimental data is 0.013 (see equation in Figure 4).

When sintered from calcined powder at 1400 °C all the compositions ($0 \le x \le 0.15$) showed similar microstructure with large grains and high relative density (>95%). In contrast, when attempting to create pellets with controlled porosity to be used for testing, Ga doping improved considerably the sinterability of the samples (Figure 5). The pellets were prepared by mixing as-sintered powder (previously ball milled) with spherical glassy carbon (20% by weight) in acetone, followed by the evaporation of the acetone and uniaxial pressing. The pellets containing carbon were fired as explained in the Experimental Section, at 1390 °C, for 6 h. The relative density of the pellets after firing is plotted against their Ga content in Figure 5, and a typical example of microstructure obtained by using this procedure is given in Figure 6. As the doping level of Ga increases, the relative density of the samples increases, the difference between the undoped composition and the one with x = 0.15 being 16%. Probably the enhanced sintering of the Ga doped samples (notice that even as little as 3% Ga makes an important impact

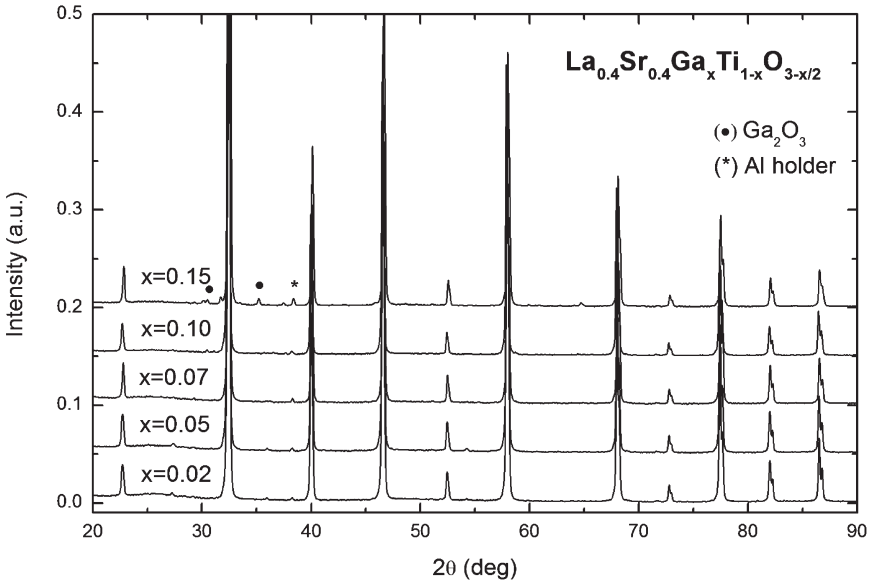

Figure 3. X-ray powder diffraction patterns recorded at room temperature in reflection mode for samples with different Ga content.

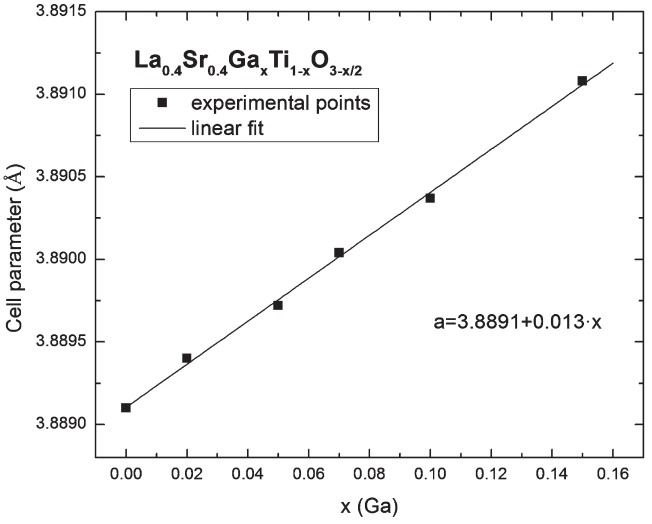

Figure 4. Refined cell parameters vs Ga doping. The errors are smaller than the points.

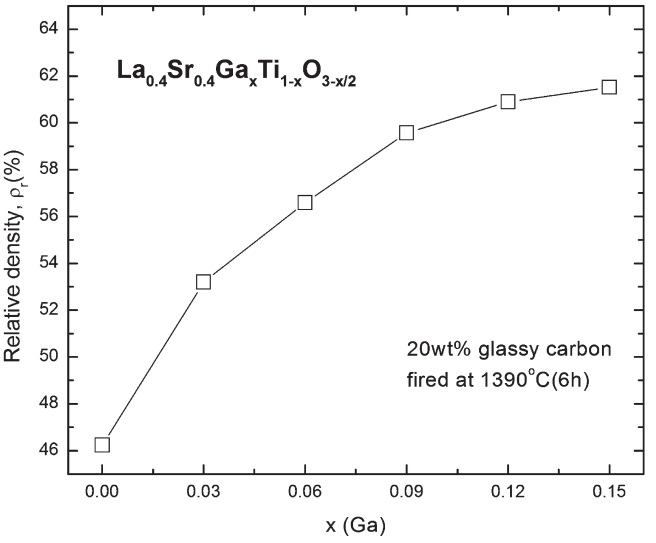

Figure 5. Relative density of pellets against Ga content. The pellets contained the same amount of pore former (20% glassy carbon) and were fired slowly to 1390 °C for 6 h. The real density was calculated by geometry, and the theoretical density by using the corresponding cell parameters.

as well) is due to the introduction of vacancies in the oxygen lattice, which together with the high A-site deficiency help ionic diffusion. This behavior was taken into account when preparing samples used in testing. The starting amount of pore former was adjusted so that the resulted pellets had a relative density between 60 and 65% over the compositional range.

3.2. Oxygen Deficiency. *3.2.1. A-Site Doping.* Various members of the solid solution $SrTiO_3$—$La_{2/3}TiO_3$ have been found to possess properties suitable for applications such as solid oxide fuel cells anodes[2,3,22] or radiation resistant materials.[23] Following this interest, several structural characterization studies of the $La_xSr_{1-3x/2}TiO_3$ system were published.[24−26] It was found that for $0 \leq x \leq 0.4$ the structure is cubic, followed by a tetragonal distortion for $0.4 < x \leq 0.55$, leading to an orthorhombic structure for $0.55 < x \leq 0.67$, for temperatures above 300 K.[25] Not only is $x \sim 0.4$ the composition after which the cubic structure converts to tetragonal but it also is the point after which A-site vacancy ordering starts occurring.[24,25] This is probably because the concentration of A-site vacancies $(x/2)$ keeps increasing with x and reaches a critical concentration somewhere close to $x = 0.4$, when the abundance of the vacancies is too high and they start associating. For $x > 0.40$—0.45, the vacancies are known to order in at least one dimension, forming a layered structure with vacant sites concentrated in alternate layers.[25,27,28]

The oxygen deficiency for some of the members belonging to this solid solution, measured on oxidation after a reduction process at 1000 °C (20 h) is presented in Figure 7. The oxygen deficiency increases gradually with doping, until $x = 0.4$, after which it starts declining.

The fact that La doping significantly promotes reduction can be explained in various ways. Most likely, the large number of

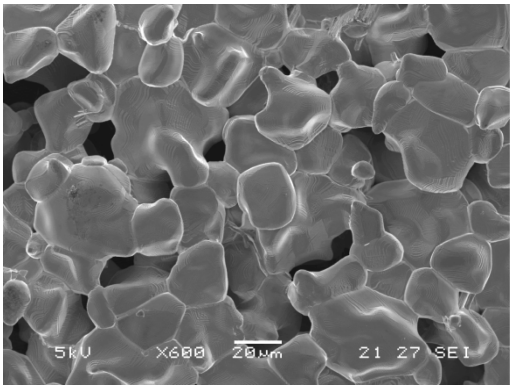

Figure 6. SEM image of a $La_{0.4}Sr_{0.4}Ga_{0.05}Ti_{0.95}O_{2.975}$ pellet with ~40% porosity.

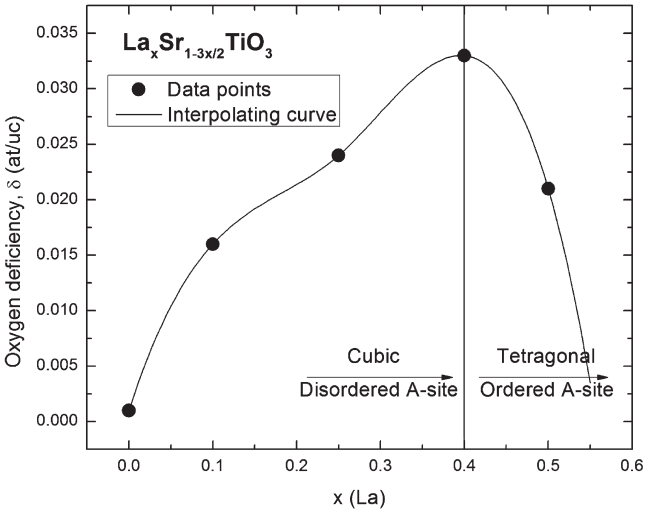

Figure 7. Oxygen deficiency vs La doping measured on ~60% dense pellets on oxidation after a reduction carried out at 1000 °C for 20 h.

V_A'' formed through doping reduces the number of intrinsic Schottky defects, pushing eq 5 to the left and thus reducing $V_O^{\cdot\cdot}$. For a given pO_2, eq 6 shifts left to oppose the change, facilitating the removal of lattice oxygen by the reducing gas, and the associated generation of free electrons.

$$A_A^x + O_O^x \leftrightarrow AO + V_A'' + V_O^{\cdot\cdot} \quad (5)$$

$$\frac{1}{2}O_2 + 2e' + V_O^{\cdot\cdot} \leftrightarrow O_O^x \quad (6)$$

Another possible explanation for the positive effect that La doping has on the reduction of the material is related to the way oxide ions travel through the bulk. As explained in the introduction, when migrating, the oxide ion must pass through the triangle described by the two A-site ions and the B-site ion (see Figure 1c). However, in this case, a large number of A-sites are vacant and therefore the oxide ion might not be required to pass through a triangle shaped bottleneck. Obviously, at some point, when the number of the A-site vacancies is too high, the presence of a large number of A-site vacancies will inhibit the formation of oxygen vacancies rather than promote their formation. This is because the perovskite structure will not tolerate a high number of A-site and oxygen vacancies at the same time. This is exactly what Figure 7 shows: after $x \sim 0.4$ the concentration of A-site vacancies is too high and they start ordering such that they distort the structure and limit the number of achievable oxygen vacancies on reduction.

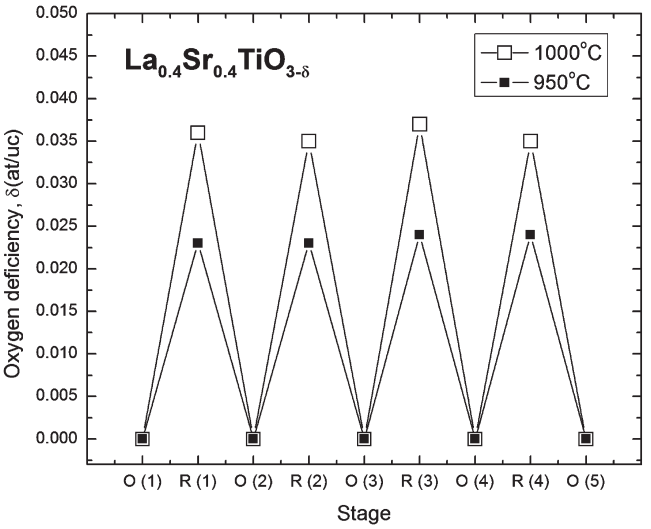

Figure 8. Oxygen deficiency at different stages of redox cycling (O-after a complete oxidation, R-after a complete reduction), carried out at two different temperatures, 950 and 1000 °C. The errors are of the size of the points.

All the tested compositions (with $x \leq 0.4$) were found to be stable during redox cycling, showing that when exposed to the same conditions the achievable oxygen deficiency is reversible. For $x = 0.4$ the oxygen deficiency achieved at different stages of the redox cycles carried out at 950 and 1000 °C is plotted in Figure 8. An interesting fact that emerges when comparing Figure 7 to Figure 8 is that the $x = 0.25$ composition reduced at 1000 °C has the same oxygen deficiency as the $x = 0.4$ composition reduced at 950 °C. This is a good example of how doping can effectively be used to lower the reduction temperature required to achieve desired properties.

3.2.2. B-Site Doping. To evaluate the effect that B-site doping has on the oxygen loss, $La_{0.4}Sr_{0.4}Ga_xTi_{1-x}O_{3-x/2}$ pellets (60−65% dense) were prepared and reduced at temperatures from 850 to 1000 °C, under 5%H_2/Ar flow. The weight loss of the samples (on reduction) is presented in Figure 9 together with the corresponding oxygen deficiency plotted on the right-hand side axis.

As expected, the weight loss increases with Ga doping, indicating that oxygen diffusion in the bulk has been indeed enhanced. However, when examining the calculated oxygen deficiencies, it becomes difficult to believe that such high values can be accommodated by a perovskite lattice that is already highly A-site deficient. This suggests that there might be another process that occurs with weight loss when reducing the samples, besides oxygen loss. Because such a behavior was not observed in the undoped composition (see for example Figure 8), this is probably an effect associated with the presence of Ga. Indeed, by looking at other Ga containing perovskites in the literature, we find that Ga can be lost from an oxide lattice when exposed to reducing conditions at high temperatures.[29,30] Two different processes that account for Ga loss have been found:[31−33]

$$Ga_2O_3(s) + 2H_2(g) \rightarrow Ga_2O(g) + 2H_2O(g) \quad (7)$$

$$Ga_2O_3(s) + 2H_2(g) \rightarrow 2GaOH(g) + H_2O(g) \quad (8)$$

It has been suggested that the most abundant species during the volatilization of Ga based oxides is Ga_2O in dry reducing

dx.doi.org/10.1021/cm103489r |*Chem. Mater.* 2011, 23, 1607–1617

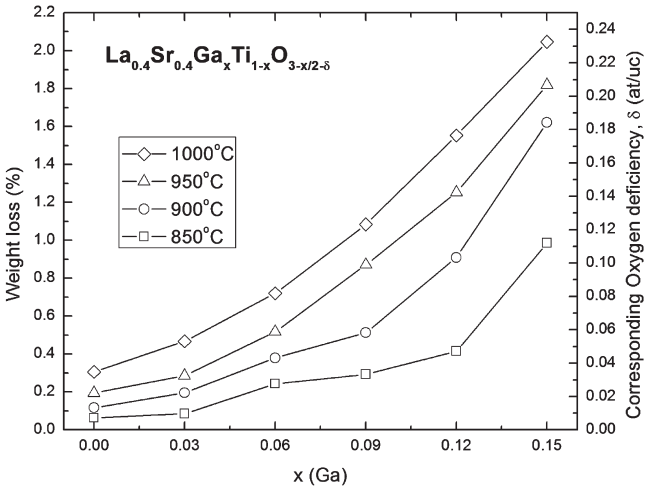

Figure 9. Weight loss measured on 60−65% dense pellets during reduction at various temperatures for 20 h, in 5%H_2/Ar flow. The corresponding oxygen deficiency is plotted on the right axis (assuming all weight loss is due to oxygen loss).

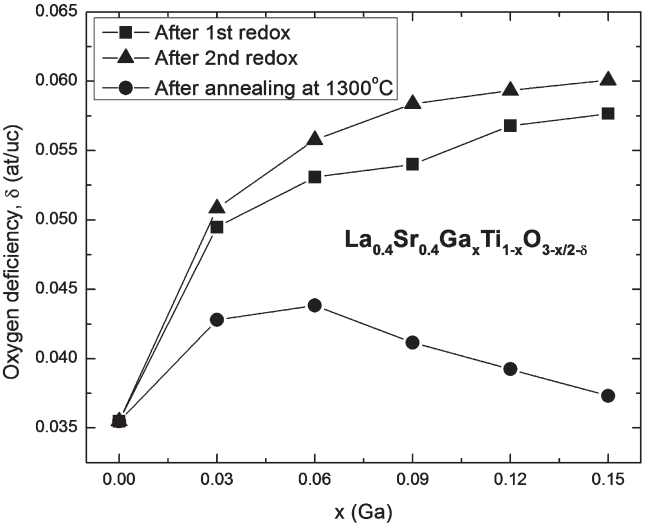

Figure 10. Oxygen deficiency vs Ga doping measured as weight gain on oxidation, in various scenarios: after a first reduction (■), after a second reduction (▲), and after an annealing at 1300 followed by a reduction (●). The samples used were 60−65% dense pellets. The reduction steps were carried out in continuous 5%H_2/Ar flow at 1000 for 20 h.

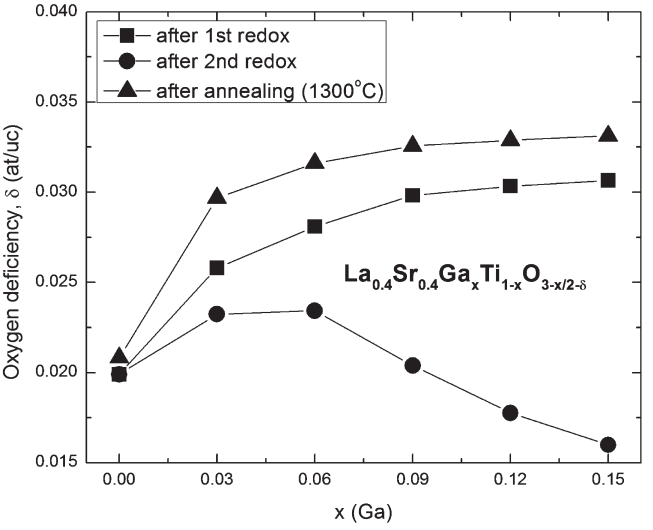

Figure 11. Oxygen deficiency vs Ga doping measured as weight gain on oxidation, in various scenarios: after a first reduction (■), after a second reduction (▲), and after an annealing at 1300 followed by a reduction (●). The samples used were 60−65% dense pellets. The reduction steps were carried out in continuous 5%H_2/Ar flow at 950 °C for 20 h.

conditions,[31] and GaOH if water is present in the reducing gas.[32] However, these studies do not rely on direct observation of the species but are rather anticipated from indirect methods and thermodynamic calculations.

To find the true oxygen deficiency of the Ga doped samples in reducing conditions and the magnitude of the Ga loss, a redox cycle was performed at 1000 °C. During the first stage, the reducing atmosphere will cause the removal of both oxygen and Ga from the structure. In the second stage the materials will be exposed to air, thus refilling the oxygen vacancies with oxide ions and enabling the calculation of the true oxygen deficiency of the samples. The amount of Ga that had been lost in the first stage can then be calculated by difference. The oxygen deficiency of the samples determined in this way after redox cycling at 950 and 1000 °C are plotted against initial Ga content in Figure 10 and Figure 11, respectively. The number of starting and remaining Ga ions per formula unit is listed in Table 1.

At both temperatures Ga doping greatly promotes oxygen loss from the structure, as anticipated (Figure 10 and Figure 11). However, Table 1 shows that the higher the initial Ga content, the higher the magnitude of Ga loss. Surprisingly, this situation changes during the second redox cycle when no further change in Ga stoichiometry is observed (3rd column in Table 1) and the oxygen deficiency of the samples slightly increases (▲ plot in Figure 10 and Figure 11). In Figure 12 the changes in oxygen stoichiometry with temperature and Ga doping can be compared. Ga doping greatly improves the achievable oxygen deficiency, especially at higher temperatures. Oxygen deficiency because of Ti^{4+} being reduced to Ti^{3+} is roughly 3 times higher at 1000 °C than the one at 900 °C. It is interesting to note here the effectiveness of Ga^{3+} in making the titanate easier to reduce. In Figure 13 the effect of doping Ga and Al on the B-site of $La_{0.4}Sr_{0.4}TiO_3$ can be compared in terms of achievable oxygen deficiency. Al doping has an opposite effect on reduction compared to Ga, probably because of the stronger bond with O and high preference for 6-fold coordination. Figure 13 suggests the following ranking of B-site cations in terms of promoting reduction: $Al^{3+} < Ti^{4+} < Ga^{3+}$.

Another implication of Ga doping and the subsequent enhanced reduction is the high number of the oxygen vacancies being created, which could support oxide ion conduction. It is known that an oxygen deficiency of 0.150 atoms per formula unit is enough to ensure a high ionic conductivity of 0.1 S cm^{-1} in doped lanthanum gallates.[7] When reduced at 1000 °C, the number of vacancies per formula unit varies in the range $0.035 \leq x/2 + \delta \leq 0.135$ because $0 \leq x \leq 0.15$ and $0.035 \leq \delta \leq 0.060$ (Figure 10). When reduced at 900 °C, however, these values are smaller: $0.012 \leq x/2 + \delta \leq 0.080$ (Figure 12), but nonetheless very high compared to other perovskite oxides.

The loss of Ga during reduction is most likely due to the incapacity of the perovskite lattice to accommodate such a high number of vacancies on both A-site and O-site at the same time. In oxidized form the Ga doped samples already possess some

dx.doi.org/10.1021/cm103489r |*Chem. Mater.* 2011, 23, 1607–1617

Table 1. Change in Ga Stoichiometry (x) after Various Redox Cycles for $La_{0.4}Sr_{0.4}Ga_xTi_{1-x_i}O_{3-x/2}$[a]

initial x_i	after 1st redox, x	after 2nd redox, x	after annealing and 3rd redox, x
0.03	0.028	0.028	0.027
0.06	0.052	0.052	0.049
0.09	0.073	0.073	0.065
0.12	0.091	0.091	0.082
0.15	0.107	0.107	0.099

[a] A redox cycle consists of a reduction step (1000 °C, 20 h) and an oxidation step (1000 °C, 12 h). The annealing was carried out at 1300 °C (20 h).

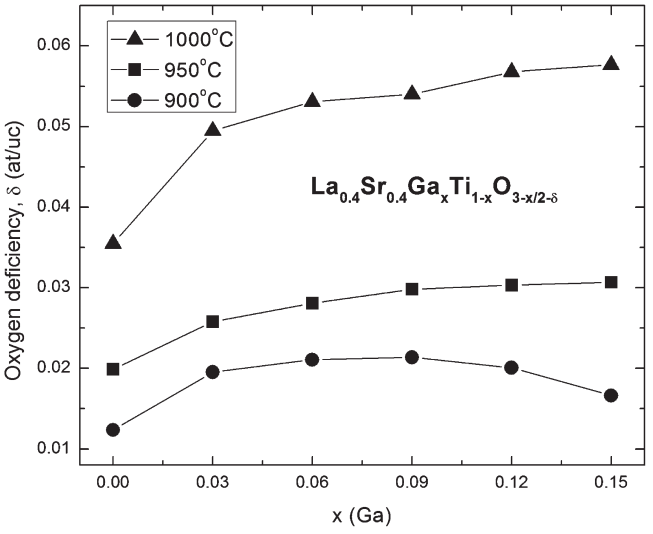

Figure 12. Change in oxygen deficiency δ with x in $La_{0.4}Sr_{0.4}Ga_x$-$Ti_{1-x}O_{3-x/2-\delta}$ at various temperatures. δ was calculated from the oxygen uptake on oxidation after the pellets (60−65% dense) were pre-reduced at (●) 900, (■) 950, and (▲) 1000 °C, respectively.

oxygen vacancies, besides the large number of A-site vacancies ($\mathbf{La_{0.4}Sr_{0.4}}Ga_xTi_{1-x}\mathbf{O_{3-x/2}}$; $0 < x < 0.15$). When exposed to reducing conditions more oxygen vacancies are created: $La_{0.4}Sr_{0.4}Ga_xTi_{1-x}\mathbf{O_{3-x/2-\delta}}$ ($0 < x < 0.15$, $0.035 < \delta < 0.06$, Figure 10). By exsolving some B-site cations (as oxides or reduced oxides) from the perovskite lattice, the occupancy on the A-site and on the O-site will increase, thus making the system more stable.[2] This mechanism is supported by our previous work in which we showed that the undoped composition can be forced to grow submicrometer reduced TiO_2 crystals (Magneli phases) on the main grains when subject to extreme reducing conditions.[2] However, because the Ga based species that form in reducing conditions are volatile (eq 7 and 8), no exsolutions are observed on the grains (by means of SEM). The samples also retained their crystal symmetry after Ga loss and no secondary phase was observed by XRD. The proposed mechanism is in good agreement with the fact that we observed the same values of Ga stoichiometry when the redox cycle was performed either at 950 or 1000 °C and also explains well why Ga loss increases with Ga doping. The higher the initial Ga content, the higher the overall deficiency of the perovskite's lattice and therefore the less stable, making it more prone to exsolve B-site oxides.

However it is not easy to explain why even slightly doped samples (3% Ga) exhibit some Ga loss. This might be due to the fact that Ga based oxides are probably not stable enough as solids

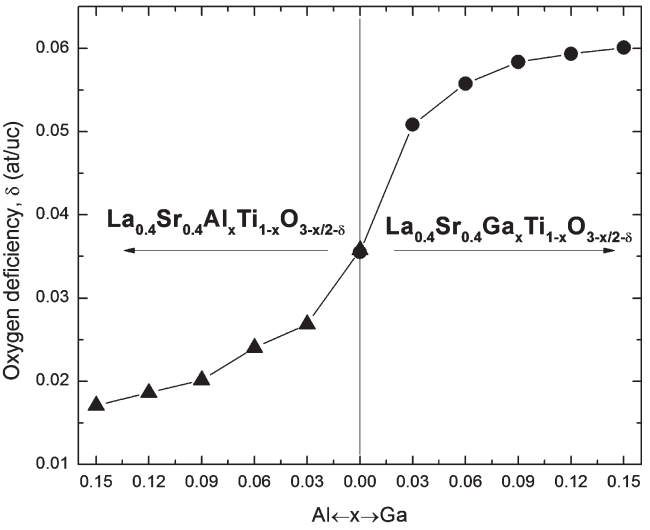

Figure 13. Oxygen deficiency δ as a function of x in $La_{0.4}Sr_{0.4}Al_x$-$Ti_{1-x}O_{3-x/2-\delta}$ and $La_{0.4}Sr_{0.4}Ga_xTi_{1-x}O_{3-x/2-\delta}$. The oxygen deficiency was calculated using the oxygen uptake on oxidation of pellets (60−65% dense) previously pre-reduced in 5%H_2/Ar at 1000 °C for 20 h.

at low pO_2 and high temperature, regardless of the oxide system they are part of.[33,34] Therefore another mechanism accounting for the observed Ga loss can be envisaged. It seems possible that the Ga ions present on the surface will be lost in reducing conditions, and the rate of their loss is controlled by their diffusion to the surface through a (thin) Ga depleted perovskite layer.

To decide which mechanism of the two proposed above has the most influence on Ga loss, several experiments were performed. To see if Ga loss is controlled by the Ga ions reaching the surface of the grains, some of the samples that lost Ga were annealed in air at 1300 °C for a long time (20 h). This annealing step provides the system with sufficient energy to rearrange its structure and thus for the Ga ions to repopulate the Ga-depleted layer covering the grains. If this happens, we should be able to record again Ga loss during reduction. Therefore, after this annealing step the samples were reduced and oxidized again to calculate their oxygen deficiency and remaining Ga stoichiometry. The results showing the oxygen deficiency of the samples are plotted in Figure 10 (redox at 1000 °C) and Figure 11 (redox at 950 °C) while the corresponding Ga stoichiometry is listed in Table 1. It is obvious from these data that the annealing step had a profound influence on the properties of the samples, triggering again Ga loss during reduction, decreasing the achievable oxygen deficiencies and thus suggesting that Ga loss is largely controlled by Ga diffusion to the surface of the grains. To further test this premise, a TGA analysis was performed on a fine powder with 5% Ga (Figure 14). However, no clear evidence was found that an increased specific surface area would increase Ga loss, as the calculated change in stoichiometry from $La_{0.4}Sr_{0.4}Ga_{0.05}Ti_{0.95}$-$O_{3-\delta'}$ to $La_{0.4}Sr_{0.4}Ga_{0.044}Ti_{0.95}O_{3-\delta''}$ was similar the one listed for porous pellets in Table 1.

3.2.3. A and B-Site Doping. To decide if Ga loss on reduction can be diminished by decreasing the A-site deficiency (as suggested by the first proposed mechanism), samples with higher A-site occupancy were doped with Ga and analyzed as previously explained to find their changes in oxygen stoichiometry and Ga loss on reduction. The Ga stoichiometry after Ga loss found for

dx.doi.org/10.1021/cm103489r |*Chem. Mater.* 2011, 23, 1607–1617

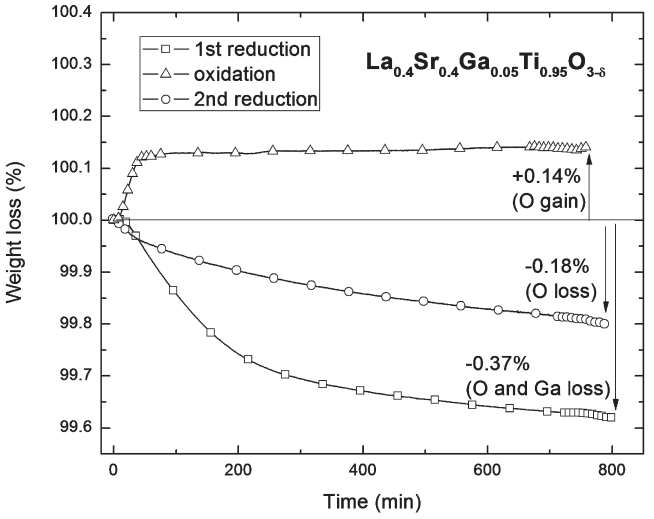

Figure 14. TGA analysis showing the weight variation with time of a $La_{0.4}Sr_{0.4}Ga_{0.05}Ti_{0.95}O_{2.975}$ sample during a redox cycle at 950 °C. Reduction was carried out in flowing 5%H2/Ar, while oxidation in flowing air.

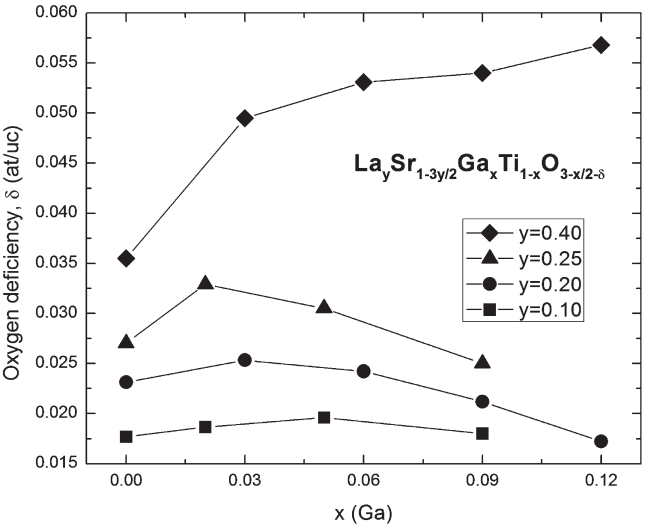

Figure 15. Change in oxygen deficiency δ as a function of x and y in $La_ySr_{1-3y/2}Ga_xTi_{1-x}O_{3-x/2-\delta}$. The oxygen deficiency was calculated using the oxygen uptake on oxidation of pellets (60−65% dense) previously pre-reduced in 5%H_2/Ar at 1000 °C for 20 h.

$La_ySr_{1-3y/2}Ga_xTi_{1-x}O_{3-x/2}$ when $y = 0.25$ or $y = 0.20$ was almost identical to the one found for the same x, for $y = 0.40$ as listed in Table 1. For $y = 0.10$ Ga loss decreased slightly but not by very significant amounts. On the other hand, the decrease of A-site deficiency caused an important decrease in the achievable oxygen deficiency on reduction (Figure 15). The value of the A-site deficiency affects the shape of the curves presented in Figure 15. For $y < 0.40$, δ does not increase continuously with Ga doping, but shows a maximum, after which it decreases as Ga doping increases. This might be understood in the following way. When Ga is lost, a layer of Ga-depleted titanate having higher A-site occupancy will cover the grains. This layer probably controls the oxygen exchanged by the bulk of the sample which is responsible for most of the oxygen deficiency observed. However, the higher the A-site occupancy of this layer, the worse its oxygen transport properties will be (Figure 7). This mechanism explains as well the observed trend in oxygen deficiency after the annealing process (Figure 10 and Figure 11), which clearly resembles the behavior of samples with low A-site deficiency (Figure 15). It seems likely that the sample with $y = 0.40$ has a sufficiently high starting A-site deficiency that even after Ga loss and its corresponding decrease of this deficiency will be able to promote a good oxygen transport.

3.3. Total Conductivity. To study the effect of doping on total conductivity, samples having 60−65% relative density were prepared, pre-reduced at 1000 °C for 20 h in 5%H_2/Ar flow, and heated to 880 °C in 5%H_2/Ar. All the samples showed high conductivity and a metallic type behavior after a semiconductor to metallic transition around 100 °C (Figure 17). Conductivity as a function of doping just after heating the samples to 880 °C and after a dwell time of 12 h is presented in Figure 16. The decrease of the conductivity is most likely due to the fact that the samples were pre-reduced in dry 5%H_2/Ar where pO_2 is lower than in the testing jig, due mainly to lower humidity (during prereduction $pO_2 \sim 10^{-20}$atm, during testing $pO_2 \sim 10^{-18}$atm compared at the same temperature of ~900 °C). Thus, the samples will attempt to re-equilibrate to the new pO_2/pH_2O conditions.

As anticipated from oxygen deficiency experiments, doping improves conductivity significantly. The resemblance between

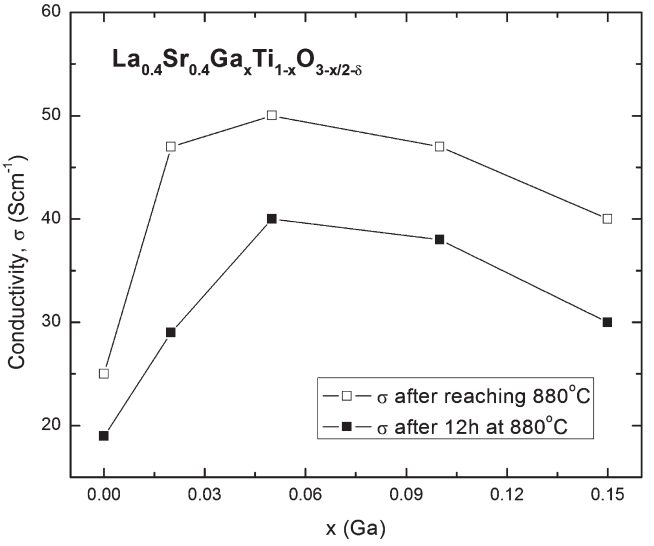

Figure 16. Conductivity (σ) as a function of composition (x) in $La_{0.4}Sr_{0.4}Ga_xTi_{1-x}O_{3-x/2-\delta}$ measured on 60−65% dense pellets, previously reduced at 1000 °C (20 h) in 5%H_2/Ar. (□) shows the conductivity just after the samples reached measuring temperature (880 °C) and (■) shows the conductivity after 12 h at measuring temperature.

the plots that show the influence of doping on δ (Figure 10) and σ (Figure 16) is quite striking. This suggests that σ is indeed proportional with δ, as δ is proportional to the concentration of free electrons (eq 2) and σ is proportional with the concentration of electrons (eq 1). However, unlike the δ vs doping trend which increases continuously, the σ vs doping shows a maximum, after which a slow decrease in conductivity is observed. This must be because with doping the number of B-site ions that are able to reduce (Ti^{4+}) decreases. Therefore the percolation between Ti ions decreases with Ga doping, thus decreasing the maximum conductivity achievable. As the electronic conduction in lanthanum gallates has been reported to be very small in reducing

dx.doi.org/10.1021/cm103489r |*Chem. Mater.* 2011, 23, 1607–1617

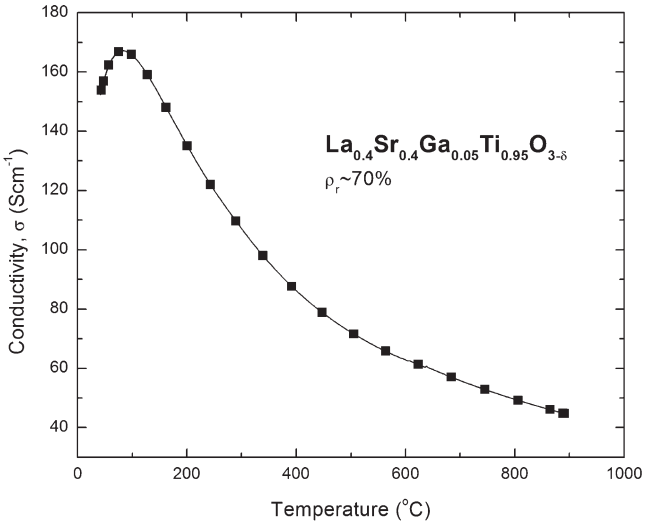

Figure 17. Conductivity as a function of temperature for a $La_{0.4}Sr_{0.4}Ga_xTi_{1-x}O_{3-x/2-\delta}$ with ~70% relative density. The sample was previously reduced at 1000 °C (20 h) in 5%H_2/Ar.

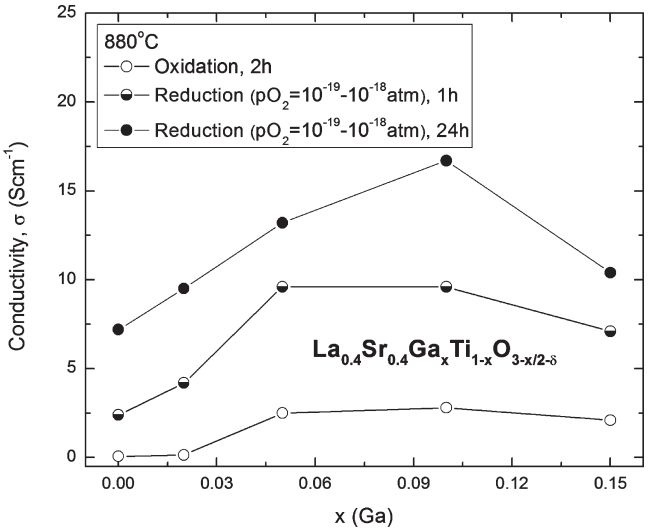

Figure 18. Conductivity (σ) as a function of composition (x) for $La_{0.4}Sr_{0.4}Ga_xTi_{1-x}O_{3-x/2-\delta}$ samples with 60−65% relative density, at different stages of a redox cycle at 880 °C. The initial conductivity is given in Figure 16 (■). The conductivity after 2 h of oxidation is marked with (○). The samples were then reduced, and the conductivity after 1 h (◒) and 24 h (●) is plotted.

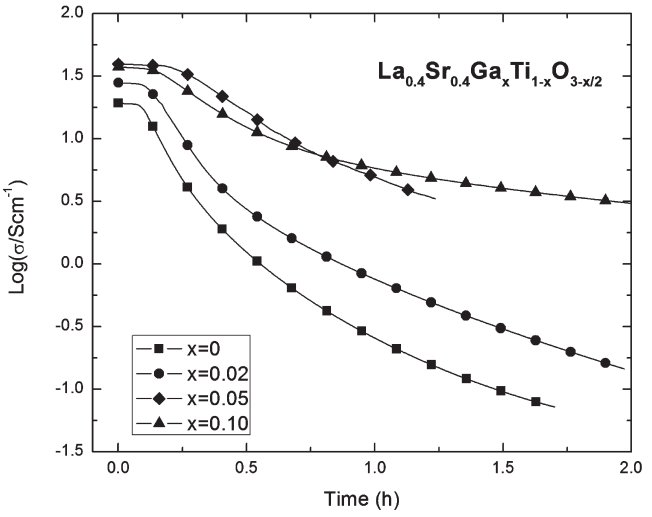

Figure 19. Log(σ) as a function of time for selected Ga-doped compositions, on oxidation (part of the experiment presented in Figure 18).

conditions,[7,8] Ga reduction will not contribute positively to conductivity. Not only does the conductivity increase with doping, but the conductivity values are quite high for ceramics. For example to achieve a conductivity of about 45 S cm^{-1} with the undoped sample, a reduction temperature of about 1250 °C was necessary, while with only 6% Ga B-site doping this conductivity can be achieved at the much lower temperature of 1000 °C, using the same gas as reducing agent (5%H_2/Ar).

To see how oxidation affects the conductivity of the samples, a redox cycle was performed. The results are plotted in Figure 18 as conductivity against composition. In the first stage, the samples having quasi-equilibrium conductivities marked with (■) in Figure 16, were oxidized for 2 h in static air. The conductivities of the samples at the end of this stage are plotted in Figure 18 with (○) symbols. It is interesting to note that while the undoped composition reached a conductivity of about 10^{-1} S cm^{-1}, the conductivity of the samples with $x > 0.10$ did not go below 2 S cm^{-1}. This suggests that the Ga doped samples are more resistant to oxidation probably because of the effect that Ga has of stabilizing the formed oxygen vacancies. However, this effect might also be related to the way Ga loss takes place. According to the second proposed mechanism, a Ga-depleted layer will cover the grains. This layer might act as a barrier for oxygen exchange, thus trapping the reduced states in the core of the grains which in turn will sustain some electronic conduction even in oxidizing conditions.

The different behavior on oxidation between the undoped and slightly doped samples on one hand and the samples with higher Ga content on the other hand can be seen better in Figure 19 where Log(σ) as a function of time is plotted. The 2% Ga doped sample tends to oxidize fast, much like the undoped sample. The behavior of the sample with 5% Ga resembles more to the 10% doped one which appears to form a stable plateau of conductivity that will not go below 1 S cm^{-1} readily. For the second stage of the redox cycle the samples were reduced using a continuous flow of 5%H_2/Ar. The conductivity values reached after 1 h and 24 h of reduction are plotted against composition in Figure 18, and conductivity against time for some selected samples is plotted in Figure 20. The final conductivity of the samples is in good agreement with the values anticipated from oxygen deficiency (Figure 12). Because the oxygen deficiency of the series is roughly 3 times lower when reduced at 900 compared to when reduced at 1000, the conductivity is expected to differ by this factor as well (according to eq 1). Indeed, if we divide the conductivity values presented in Figure 16 (□) by 3 we get conductivity values close to the ones presented in Figure 18 (●).

It is apparent from Figure 18 that the samples achieve most of their final conductivity just after 1 h of reduction. This might be due to a combined effect of doping and microstructure. Because the microstructure is very porous (35−40% porosity) the contact surface between the reducing gas and the solid phase is very high; therefore, a larger fraction of the material will reduce faster. However, because of the large number of the grain

dx.doi.org/10.1021/cm103489r |*Chem. Mater.* 2011, 23, 1607–1617

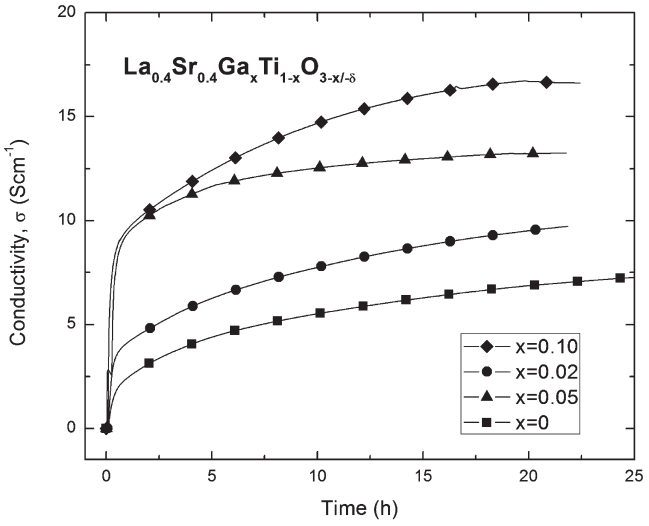

Figure 20. Conductivity as a function of time on reduction of selected Ga-doped samples (part of the experiment presented in Figure 18).

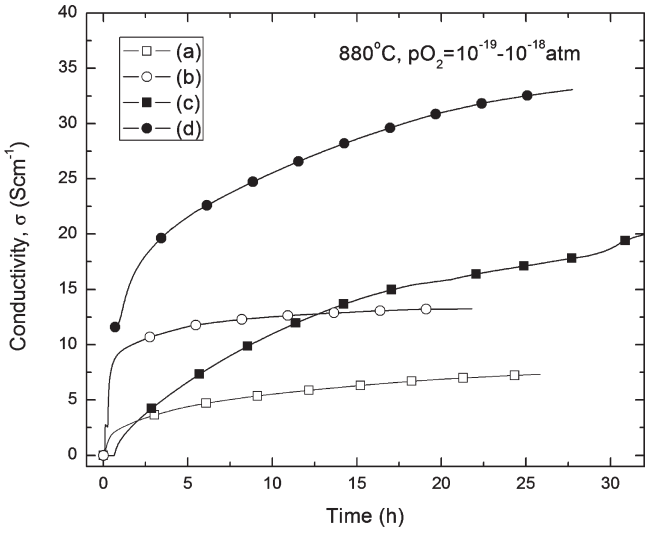

Figure 21. Conductivity as a function of time on reduction of $La_{0.4}Sr_{0.4}Ga_{0.05}Ti_{0.95}O_{2.975-\delta}$ pellets in various scenarios, compared to the undoped composition, $La_{0.4}Sr_{0.4}TiO_{3-\delta}$. (a) the oxidized form of the undoped composition with ~60% relative density; (b) the oxidized form of $La_{0.4}Sr_{0.4}Ga_{0.05}Ti_{0.95}O_{2.975-\delta}$ with ~60% relative density; (c) the oxidized form of $La_{0.4}Sr_{0.4}Ga_{0.05}Ti_{0.95}O_{2.975-\delta}$ with ~70% relative density; (d) a briefly oxidized (1 h) $La_{0.4}Sr_{0.4}Ga_{0.05}Ti_{0.95}O_{2.975-\delta}$ with ~70% relative density.

boundaries that exists in a ceramic with high porosity, the final conductivity achieved will not be rather low. This behavior is better illustrated in Figure 21 where the evolution of conductivity with time has been recorded during the reduction of $La_{0.4}Sr_{0.4}Ga_{0.05}Ti_{0.95}O_{2.975}$ samples.

The conductivity of the samples with about ~60% relative density ($La_{0.4}Sr_{0.4}Ti_{0.95}O_3$ and $La_{0.4}Sr_{0.4}Ga_{0.05}Ti_{0.95}O_{2.975}$) follow the same trend showing a fast and significant increase within 1−2 h of reduction. On the contrary, the sample with ~70% relative density ($La_{0.4}Sr_{0.4}Ga_{0.05}Ti_{0.95}O_{2.975}$) shows a very slow increase in conductivity with time, but will eventually reach a conductivity that is almost double the conductivity of the sample having 60% density.

4. CONCLUSIONS

The study was undertaken to design perovskites exhibiting high n-type conductivity. Our doping strategy was aimed at increasing the bulk mobility and stability of the oxygen vacancies to allow a higher rate and extent of the reduction in these materials, which in turn will increase the concentration of charge carriers. The validity of this approach was evaluated by measuring the conductivity and oxygen deficiency on reduction as a function of Ga doping in $La_{0.4}Sr_{0.4}Ga_xTi_{1-x}O_{3-x/2-\delta}$ ($0 < x < 0.15$).

Both oxygen deficiency and conductivity greatly improve with Ga doping. For example, after a typical reduction process carried out at 1000 °C in 5%H_2/Ar, we found δ to increase from 0.035 to 0.060 when Ga stoichiometry was varied from $x = 0$ to $x = 0.15$. The corresponding conductivity values also increase with doping and show a maximum conductivity of 50 S cm^{-1}, measured at 880 °C in 5%H_2/Ar on a ~62% dense pellet. To the best of our knowledge the conductivity values that we measured in this system are the highest ever reported for strontium titanate based materials equilibrated at fuel conditions, especially considering the high porosity we deliberately induced in our samples. For example, when subject to the same reducing conditions as used in this study (1000 °C, 5%H_2/Ar), (Sr,Y)TiO_3 materials show a conductivity of only ~10 S/cm^{-1} measured at 810 °C,[35] while (La,Ca)$Cr_{0.2}Ti_{0.8}O_3$ dense samples show a conductivity below 10 S cm^{-1}.[36]

The high concentration of oxygen vacancies achieved at low pO_2, together with the vacancies generated by doping ($0.035 < x/2 + \delta < 0.135$) suggests that these compounds might exhibit some ionic conduction and therefore might be mixed ionic and electronic conductors. Ga doping also promotes a fast reduction of the samples and significantly increases the stability of the reduced phase in oxidizing conditions, at high temperatures, as suggested by conductivity data.

Although the materials were found to preserve their cubic structure and microstructure throughout testing at various temperatures and oxygen partial pressures, some Ga loss was observed during reduction. However, after a first redox is performed, no further change in Ga stoichiometry is observed, and the properties of the materials slightly improve. Two possible explanations were suggested and discussed to account for the way Ga is lost from the perovskite lattice in reducing conditions.

AUTHOR INFORMATION

Corresponding Author

*E-mail: dn67@st-andrews.ac.uk.

ACKNOWLEDGMENT

The authors acknowledge the SOFC600 European project SES6-2006-020089 and the SUPERGEN XIV - Delivery of Sustainable Hydrogen project for financial support. D.N. also thanks Dr. Paul Connor and Dr. David Miller from St. Andrews for help with conductivity measurements.

REFERENCES

(1) Ishihara, T. In *Perovskite Oxide for Solid Oxide Fuel Cells*; Ishihara, T., Ed.; Springer: New York, 2009.

(2) Neagu, D.; Irvine, J. T. S. *Chem. Mater.* **2010**, *22*, 5042−5053.

(3) Slater, P. R.; Fagg, D. P.; Irvine, J. T. S. *J. Mater. Chem.* **1997**, *7*, 2495–2498.

(4) Blennow, P.; Hagen, A.; Hansen, K.; Wallenberg, L.; Mogensen, M. *Solid State Ionics* **2008**, *179*, 2047–2058.

(5) Hui, S.; Petric, A. *J. Eur. Ceram. Soc.* **2002**, *22*, 1673–1681.
(6) Ishihara, T.; Matsuda, H.; Azmi bin Bustam, M.; Takita, Y. *Solid State Ionics* **1996**, *86*−*88*, 197–201.
(7) Ishihara, T. In *Perovskite Oxide for Solid Oxide Fuel Cells*; Ishihara, T., Ed.; Springer: New York, 2009.
(8) Iwahara, H. In *Perovskite Oxide for Solid Oxide Fuel Cells*; Ishihara, T., Ed.; Springer: New York, 2009.
(9) Kharton, V.; Marques, F.; Atkinson, A. *Solid State Ionics* **2004**, *174*, 135–149.
(10) Kilner, J. A.; Berenov, A.; Rossiny, J. In *Perovskite Oxide for Solid Oxide Fuel Cells*; Ishihara, T., Ed.; Springer: New York, 2009.
(11) Mogensen, M.; Lybye, D.; Bonanos, N.; Hendriksen, P.; Poulsen, F. *Solid State Ionics* **2004**, *174*, 279–286.
(12) Slater, P. R.; Irvine, J. T. S.; Ishihara, T.; Takita, Y. *J. Solid State Chem.* **1998**, *139*, 135–143.
(13) Yashima, M. In *Perovskite Oxide for Solid Oxide Fuel Cells*; Ishihara, T., Ed.; Springer: New York, 2009.
(14) Yashima, M. *Solid State Ionics* **2008**, *179*, 797–803.
(15) Irvine, J. In *Perovskite Oxide for Solid Oxide Fuel Cells*; Ishihara, T., Ed.; Springer: New York, 2009.
(16) Tao, S.; Irvine, J. T. S. *Nat. Mater.* **2003**, *2*, 320–323.
(17) Escudero, M.; Irvine, J.; Daza, L. *J. Power Sources* **2009**, *192*, 43–50.
(18) Islam, M. S.; Davies, R. A. *J. Mater. Chem.* **2004**, *14*, 86.
(19) Ruiz-Morales, J. C.; Canales-Vázquez, J.; Savaniu, C.; Marrero-López, D.; Zhou, W.; Irvine, J. T. S. *Nature* **2006**, *439*, 568–571.
(20) Shannon, R. D. *Acta Crystallogr., Sect. A* **1976**, *32*, 751–767.
(21) Kim, D. *J. Am. Ceram. Soc.* **1989**, *72*, 1415–1421.
(22) Savaniu, C.; Irvine, J. T. S. *J. Mater. Chem.* **2009**, *19*, 8119–8128.
(23) Smith, K. L.; Lumpkin, G. R.; Blackford, M. G.; Colella, M.; Zaluzec, N. J. *J. Appl. Phys.* **2008**, *103*, 083531.
(24) Battle, P.; Bennett, J. E.; Sloan, J.; Tilley, R. J. D.; Vente, J. F. *J. Solid State Chem.* **2000**, *149*, 360–369.
(25) Howard, C.; Lumpkin, G.; Smith, R.; Zhang, Z. *J. Solid State Chem.* **2004**, *177*, 2726–2732.
(26) Thomas, B. S.; Marks, N. A.; Harrowell, P. *Phys. Rev. B* **2006**, 74.
(27) Kendrick, E.; Islam, M.; Slater, P. *Solid State Ionics* **2005**, *176*, 2975–2978.
(28) Slater, P. R.; Irvine, J. T. S. *Solid State Ionics* **1999**, *124*, 61–72.
(29) Yamaji, K.; Horita, T.; Ishikawa, M.; Sakai, N.; Yokokawa, H. *Solid State Ionics* **1998**, *108*, 415–421.
(30) Yamaji, K.; Horita, T.; Ishikawa, M.; Sakai, N.; Yokokawa, H. *Solid State Ionics* **1999**, *121*, 217–224.
(31) Butt, D. P.; Park, Y.; Taylor, T. N. *J. Nucl. Mater.* **1999**, *264*, 71–77.
(32) Stanislowski, M.; Seeling, U.; Peck, D.; Woo, S.; Singheiser, L.; Hilpert, K. *Solid State Ionics* **2005**, *176*, 2523–2533.
(33) Stevenson, J. W.; Armstrong, T. R.; Pederson, L. R.; Li, J.; Lewinsohn, C. A.; Baskaran, S. *Solid State Ionics* **1998**, *113*−*115*, 571–583.
(34) Yamaji, K.; Negishi; Horita; Sakai; Yokokawa *Solid State Ionics* **2000**, *135*, 389–396.
(35) Fu, Q.; Mi, S.; Wessel, E.; Tietz, F. *J. Eur. Ceram. Soc.* **2008**, *28*, 811–820.
(36) Vashook, V.; Vasylechko, L.; Ullmann, H.; Guth, U. *Solid State Ionics* **2003**, *158*, 317–325.